

SUPPLEMENTARY INFORMATION

Low-Spin and Spin-Crossover Iron(II) Complexes with Pyridyl-benzimidazole Ligands: Synthesis, Structural, Magnetic and Solution study

Barbora Brachňaková,^a Júlia Adamko Kožíšková,^b Jozef Kožíšek,^b Eva Melníková,^c Miroslav Gál,^c Radovan Herchel,^d Tibor Dubaj,^b and Ivan Šalitros^{*ade}

- a) Department of Inorganic Chemistry, Faculty of Chemical and Food Technology, Slovak University of Technology in Bratislava, Bratislava SK-81237, Slovakia, **e-mail:* ivan.salitros@stuba.sk
- b) Department of Physical Chemistry, Faculty of Chemical and Food Technology, Slovak University of Technology in Bratislava, Bratislava SK-81237, Slovakia
- c) Department of Inorganic Technology, Faculty of Chemical and Food Technology, Slovak University of Technology in Bratislava, Bratislava SK-81237, Slovakia
- d) Department of Inorganic Chemistry, Regional Centre of Advanced Technologies and Materials, Faculty of Science, Palacký University, 17. listopadu 12, 771 46 Olomouc, Czech Republic
- e) Central European Institute of Technology, Brno University of Technology, Purkyňova 123, 61200 Brno, Czech Republic

Contents

S1. Experimental section	2
S1.1 Materials.....	2
S1.2 Synthesis	2
S1.3 Single-crystal diffraction experiments.....	6
S1.4 Magnetic measurements.....	6
S1.5 Electrochemistry	7
S2. Spectral characterisation.....	8
S3. Supplementary structural information.....	19
S4. Magnetic measurements	24
References	25

S1. Experimental section

S1.1 Materials

3,5-di-*tert*-butylbenzyl bromide, 4-*tert*-butylbenzyl chloride, FeCl₂·4H₂O, Fe(ClO₄)₂·6H₂O, Fe(CF₃SO₃)₂, Fe(BF₄)₂·6H₂O, NaBPh₄, ethanol, acetonitrile and acetone were used as received without any further purification. The starting material 2,6-bis(1*H*-benzimidazol-2-yl)pyridine and 2-(pyridin-2-yl)-1*H*-benzimidazole were prepared by published methods¹. IR spectra were measured by the ATR technique or in KBr pellets in 4000 – 400 cm⁻¹ region (Magna FTIR 750. Nicolet). Electronic spectra were recorded in the acetonitrile solutions at the concentration ≈10⁻⁵ mol dm⁻³ on Specord 250 plus Analytical Jena in the range of 800 – 200 nm. Elemental analysis of carbon, hydrogen and nitrogen was carried out by an automated analyser (Vario Micro Cube). The microcrystalline solid of complexes **1-8** were measured by Philips PW 1730/1050 (Bragg – Brentano geometry, Co-K α radiation, 40kV/35mA, range of 2 Θ 3-52°, step 0.02°) diffractometer. Synthesis of 2,6-bis(1-(3,5-di-*tert*-butylbenzyl)-1*H*-benzimidazol-2-yl)pyridine (**L1**) is described in ref. 2. Thermogravimetric analysis was carried out using a simultaneous analyzer Seiko EXSTAR 6300 (Chiba, Japan) in nitrogen purge. The measurement was performed in 30–350 °C range with temperature ramp of 5 °C/min.

S1.2 Synthesis

*Synthesis of 2,6-bis(1-(4-*tert*-butylbenzyl)-1*H*-benzimidazol-2-yl)pyridine (**L2**)*

50 cm³ two-necked round-bottom flask was charged with 2,6-bis(1*H*-benzimidazol-2-yl)pyridine (1.0 g, 3.21 mmol, 1 eq), crushed KOH (1.08 g, 19.2 mmol, 6 eq) and dissolved in DMSO (20 cm³). The solution was rigorously stirred for 1 hour at RT. Next, 4-*tert*-butylbenzyl chloride (1.29 g, 6.4 mmol, 2.2 eq) was added into the flask and the white suspension was heated at 60°C for 24 hours. The reaction mixture was diluted with cold distilled water (50 cm³) and filtered off. The crude product was dissolved in acetone (100 cm³), refluxed with activated charcoal for 30 minutes, filtered off and evaporated on rotary evaporator to dryness. The white polycrystalline product was collected in 78 % yield.

¹H NMR (400 MHz, d⁶-DMSO, 25 °C, δ /ppm): 8.39 (d, J = 7.6 Hz, 2H), 8.27 (dd, J = 8.5, 7.3 Hz, 1H), 7.80 (dt, J = 9.3, 4.8 Hz, 2H), 7.73 – 7.65 (m, 2H), 7.34 (pd, J = 7.2, 1.3 Hz, 4H), 7.17 (dd, J = 5.5, 3.9 Hz, 2H), 6.76 (d, J = 1.6 Hz, 4H), 5.77 (s, 4H), 1.02 (s, 18H). ¹³C NMR (101 MHz, d⁶-DMSO, 25 °C, δ /ppm): 151.28 (d, J = 12.6 Hz), 150.55 (d, J = 12.0 Hz), 150.27 (s), 143.20 (s), 139.73 (d, J = 9.0 Hz), 137.31 (d, J = 14.2 Hz), 126.22 (d, J = 18.8 Hz), 124.33 (d, J = 12.2 Hz), 123.51 (d, J = 7.8 Hz), 121.73 (s), 121.68 (d, J = 10.7 Hz), 120.55 (d, J = 22.2 Hz), 112.27 (s), 48.40 (d, J = 9.6 Hz), 35.08 (s), 31.80 (s). Elemental analysis for C₄₁H₄₁N₅ (M_w = 603.79 g·mol⁻¹) found % (expected %): C 80.25 (81.56); N 10.72 (11.60); H 7.34 (6.84). FT-IR (ATR, $\tilde{\nu}_{\max}$ /cm⁻¹): 3053 (w, C-

H_{ar}); 2960, 2927, 2865 (w, C-H_{alif}); 1588, 1572 (m, C-C_{ar} a C_{ar}-N). UV-VIS (acetonitrile, λ/nm, 1.10⁻⁵ mol.L⁻¹): 327 (n → π*).

Synthesis of 1-(4-tert-butylbenzyl)-2-pyridine-2-yl-1H-benzimidazol (L3)

2-(pyridin-2-yl)-1H-benzimidazole (1.0 g, 5.1 mmol, 1 eq) and excess of crushed KOH (1.18 g, 21 mmol, 4 eq) were dissolved in DMSO (15 cm³) and stirred for 30 minutes at RT. Next, 4-tert-butylbenzyl chloride (1.04 g, 5.6 mmol, 1.1 eq) was added into the flask and the yellow colored suspension was heated at 60°C for 24 hours. The mixture was cooled down to RT and diluted with distilled cold water (100 cm³). The light-yellow precipitated product was vacuum filtered, washed with distilled water and dissolved in acetone. Further dissolving in acetone, treatment with activated charcoal and recrystallisation afforded product as beige polycrystalline powder in 72 % yield. Second crystallization from acetone provides colorless polycrystalline powder in 15 % yield.

¹H NMR (400 MHz, d⁶-DMSO, 25 °C, δ/ppm): 8.71 (ddd, *J* = 4.8, 1.7, 0.9 Hz, 1H), 8.38 (dt, *J* = 8.0, 1.0 Hz, 1H), 8.02 (td, *J* = 7.8, 1.8 Hz, 1H), 7.75 (dd, *J* = 4.8, 1.6 Hz, 1H), 7.61 – 7.56 (m, 1H), 7.52 (ddd, *J* = 7.6, 4.8, 1.2 Hz, 1H), 7.29 – 7.23 (m, 1H), 7.06 (d, *J* = 8.4 Hz, 1H), 6.20 (s, 1H), 1.18 (s, 1H). ¹³C NMR (101 MHz, d⁶-DMSO, 25 °C, δ/ppm): 150.00 (s), 149.60 (d, *J* = 4.0 Hz), 149.13 (d, *J* = 8.4 Hz), 148.76 (d, *J* = 16.8 Hz), 142.73 – 141.66 (m), 137.46 (d, *J* = 17.3 Hz), 136.41 (d, *J* = 7.1 Hz), 134.57 (d, *J* = 28.1 Hz), 126.39 (d, *J* = 13.7 Hz), 125.28 (s), 124.38 (d, *J* = 10.4 Hz), 123.29 (d, *J* = 12.5 Hz), 122.49 (d, *J* = 8.2 Hz), 119.48 (d, *J* = 22.2 Hz), 111.35 (d, *J* = 5.3 Hz), 46.81 (d, *J* = 146.1 Hz), 33.95 (d, *J* = 37.1 Hz), 30.70 (d, *J* = 63.9 Hz). Elemental analysis for C₂₃H₂₃N₃ (*M*_w = 341.45 g.mol⁻¹) found % (expected %): C 80.33 (80.90); N 12.34 (12.31); H 6.78 (6.79). FT-IR (ATR, $\tilde{\nu}_{\max}$ /cm⁻¹): 3049 (w, C-H_{ar}); 2999, 2958, 2941, 2896 (w, C-H_{alif}); 1587, 1567 (m, C-C_{ar} a C_{ar}-N). UV-VIS (acetonitrile, λ/nm, 1.10⁻⁵ mol.L⁻¹): 310 (n → π*).

Preparation of Fe(II) coordination compounds 1-8

All procedures were done in 100 ml three-necked round bottom flask under inert atmosphere and at RT (compound **1-5**) or at 70°C (compounds **6-8**). The crystals suitable for the single-crystal X-ray diffraction analysis were obtained after several days of slow evaporation of solution at RT. All ferrous compounds were characterized by FT-IR (Figure S3), UV-VIS spectroscopy (Figure S4) and elemental analysis. The phase purity of obtained crystalline or polycrystalline compounds **1-8** was investigated by powder X-ray diffraction spectroscopy (Figure S5).

Compound 1 [Fe(L1)₂](ClO₄)₂·EtOH·H₂O

100 cm³ three-necked round-bottom flask was charged with ligand **L1** (100.2 mg, 0.140 mmol, 2 eq) and dissolved in ethanol (50 cm³), stirred under the N₂ atmosphere at RT for 1 hour. Next, ethanolic solution (10 cm³) of Fe(ClO₄)₂

.6H₂O (27.8 mg, 0.077 mmol, 1.1 eq) was added. The complexation of the ligand took the place immediately and was accompanied by the color change of the solution to dark violet. The mixture was further stirred for 2 hours at RT under the N₂ atmosphere filtered off and left for slow crystallization at RT. After several days, the dark violet single-crystals were collected with a 40 % yield. Elemental analysis for C₁₀₀H₁₂₂FeN₁₀O₁₀Cl₂ (*M_w*= 1750.85 g.mol⁻¹) found % (expected %): C 67.84 (67.90); N 8.03 (8.00); H 6.94 (7.02). FT-IR (ATR, $\tilde{\nu}_{\max}/\text{cm}^{-1}$): 3060 (w, C-H_{ar}), 2954, 2904, 2865 (w, C-H_{alif}), 1601 (m, C-C_{ar} a C_{ar}-N). UV-VIS (acetonitrile, λ/nm , 1.10⁻⁵ mol.L⁻¹): 319, 353, 370, 579.

Compound 2 [Fe(L1)₂](BF₄)₂·2H₂O

Two equivalents of L1 (100.2 mg, 0.140 mmol, 2.0 eq) were dissolved in methanol (35 cm³) and stirred for 1 hour under N₂ at RT. Methanolic solution (5 cm³) with dissolved Fe(BF₄)₂·6H₂O (23.6 mg, 0.070 mmol, 1.0 eq) was added into 100 cm³ three-necked round-bottom flask contained ligand solution and sudden color change to dark violet was observed. The mixture was further stirred for 2 hours at RT under N₂ atmosphere, filtered off and left for slow crystallization at RT. After several days, small dark violet single-crystals with 36 % yield were collected. Elemental analysis for C₉₈H₁₁₄FeN₁₀B₂F₈ (*M_w*= 1661.47 g.mol⁻¹) found % (expected %): C 69.57 (70.84); N 8.08 (8.43); H 6.68 (6.92). FT-IR (ATR, $\tilde{\nu}_{\max}/\text{cm}^{-1}$): 3067 (w, C-H_{ar}), 2954, 2896, 2865 (w, C-H_{alif}), 1601 (m, C-C_{ar} a C_{ar}-N). UV-VIS (acetonitrile, λ/nm , 1.10⁻⁵ mol.L⁻¹): 319, 353, 370, 579; UV-VIS (nujol, λ/nm): 361, 555, 579.

Compound 3 [Fe(L1)₂](CF₃SO₃)₂·3EtOH

L1 (100.2 mg, 0.140 mmol, 2.0 eq) was dissolved in a mixture of acetone-ethanol (1:1, 60 cm³) and stirred at RT for 1 hour stirred under the N₂. Fe(CF₃SO₃)₂ (24.8 mg, 0.070 mmol, 1.0 eq) was dissolved in ethanol (5 cm³) and in combination with ligand solution turned color of solution to dark-violet. The mixture was further stirred for 2 hours at RT under the N₂ atmosphere. The solution was filtered off and slow crystallized at RT. Dark violet single-crystals were obtained in 41% yield after several days. Elemental analysis for C₁₀₆H₁₃₂FeN₁₀O₉F₆S₂ (*M_w*= 1924.19 g.mol⁻¹) found % (expected %): C 65.96 (66.16); N 7.10 (7.28); H 6,76 (6.91). FT-IR (ATR, $\tilde{\nu}_{\max}/\text{cm}^{-1}$): 3060 (w, C-H_{ar}), 2955, 2907, 2866 (w, C-H_{alif}), 1601, 1504 (m, C-C_{ar} a C_{ar}-N). UV-VIS (acetonitrile, λ/nm , 1.10⁻⁵ mol.L⁻¹): 218, 319, 352, 370, 579.

Compounds 4 [Fe(L2)₂](ClO₄)₂·C₃H₆O and 5 [Fe(L2)₂](CF₃SO₃)₂

L2 (100 mg, 0.165 mmol, 2.0 eq) was dissolved in a mixture methanol-acetone (1:1, 50 cm³) and stirred under the N₂ atmosphere for 1 hour at RT. Corresponding Fe(II) salt (32.9 mg of Fe(ClO₄)₂·6H₂O for 3 or 32.1 mg of Fe(CF₃SO₃)₂ for 4, 0.091 mmol, 1.1 eq) was dissolved in the ethanol (10 cm³) and added to the ligand solution. The resulting dark violet mixture was stirred at RT for 2 hours, filtered and mother liquor was submitted for the slow crystallization at RT. The dark purple single-crystals were obtained in 46 % (compound 4) and 32% (compound 5).

Compound 4: Elemental analysis for $C_{85}H_{88}FeN_{10}O_9Cl_2$ ($M_w = 1520.41 \text{ g mol}^{-1}$) found % (expected %): C 66.61 (67.15); N 9.12 (9.21); H 5.73 (5.83). FT-IR (ATR, $\tilde{\nu}_{\text{max}}/\text{cm}^{-1}$): 3060, 3030 (w, C-H_{ar}), 2958, 2902, 2867 (w, C-H_{alif}), 1603, 1514, 1503 (m, C-C_{ar} a C_{ar}-N). UV-VIS (acetonitrile, λ/nm , $1.10^{-5} \text{ mol.L}^{-1}$): 318, 352, 368, 577. Compound 5: Elemental analysis for $C_{84}H_{82}FeN_{10}O_6F_6S_2$ ($M_w = 1561.58 \text{ g.mol}^{-1}$) found % (expected %): C 64.52 (64.61); N 8.78 (8.97); H 5.15 (5.29); S 4.08 (4.11). FT-IR (ATR, $\tilde{\nu}_{\text{max}}/\text{cm}^{-1}$): 3064, 3030 (w, C-H_{ar}), 2964, 2900, 2864 (w, C-H_{alif}), 1603, 1515, 1502 (m, C-C_{ar} a C_{ar}-N). UV-VIS (acetonitrile, λ/nm , $1.10^{-5} \text{ mol.L}^{-1}$): 319, 350, 368, 577.

Compound 6 [Fe(L2)₂](BPh₄)₂

L2 (100 mg, 0.165 mmol, 2.0 eq) was dissolved in the mixture ethanol-acetone (1:1, 60 cm³) and stirred under N₂ atmosphere at RT for 30 minutes. Corresponding Fe(II) salt was prepared *in situ* from FeCl₂·4H₂O (18.1 mg, 0.091 mmol, 1.1 eq) and NaBPh₄ (56.4 mg, 0.165 mmol, 2.0 eq) in ethanol (10 cm³) and with small quantity of ascorbic acid to prevent oxidation of Fe(II). When the Fe(BPh₄)₂ solution was added, the complexation reaction had been manifested by color change to dark violet. The reaction mixture was stirred at 70°C for 2 hours, cooled down and filtered off. After two weeks of crystallization at RT, the dark purple single-crystals were collected in 67 % yield. Elemental analysis for $C_{130}H_{122}FeN_{10}B_2$ ($M_w = 1901.85 \text{ g.mol}^{-1}$) found % (expected %): C 82.01 (82.10); N 7.09 (7.36); H 6.37 (6.47). FT-IR (ATR, $\tilde{\nu}_{\text{max}}/\text{cm}^{-1}$): 3053 (w, C-H_{ar}), 2959, 2898, 2860 (w, C-H_{alif}), 1601, 1579 (m, C-C_{ar} a C_{ar}-N). UV - VIS (acetonitrile, λ/nm , $1.10^{-5} \text{ mol.L}^{-1}$): 318, 351, 368, 578.

Compound 7 [Fe(L3)₃](ClO₄)₂

L3 (100 mg, 0.293 mmol, 3.0 eq) was dissolved in the solvent mixture acetone-ethanol (1:2, 40 cm³) and heated up to 70 °C for 1 hour stirred under N₂. The corresponding Fe(ClO₄)₂·6H₂O (35.3 mg, 0.098 mmol, 1.0 eq) salt was dissolved in of the same solvent mixture (5 cm³) and promptly added into the ligand solution which caused color change to wine-red color. The reaction mixture was stirred for 2 hours, filtered and retained for the slow evaporation at RT. The single-crystals were obtained in 72 % after several days. Elemental analysis for $C_{69}H_{69}FeN_9O_8Cl_2$ ($M_w = 1279.08 \text{ g.mol}^{-1}$) found % (expected %): C 64.03 (64.79); N 9.64 (9.86); H 5.56 (5.44). FT-IR (ATR, $\tilde{\nu}_{\text{max}}/\text{cm}^{-1}$): 3068, 3031 (w, C-H_{ar}), 2960, 2904, 2867 (w, C-H_{alif}), 1602, 1514 (m, C-C_{ar} a C_{ar}-N). UV-VIS (acetonitrile, λ/nm , $1.10^{-5} \text{ mol.L}^{-1}$): 315, 525.

Compound 8 [Fe(L3)₃](BF₄)₂

The compound **8** was prepared by reaction of **L3** (50 mg, 0.146 mmol, 3.0 eq) and Fe(BF₄)₂·6H₂O (18.1 mg, 0.054 mmol, 1.1 eq) in acetone-ethanol (1:1, 30 cm³) stirred under N₂. The vine colored complex was stirred at 70 °C for 1 hour, filtered off and crystallized at RT by slow evaporation of solvent. Yield of dark pink single-crystals was 35 % after 2 weeks. Elemental analysis for $C_{69}H_{69}FeN_9B_2F_8$ ($M_w = 1253.81 \text{ g.mol}^{-1}$) found % (expected %): C 66.06 (66.10); N 9.31 (10.05); H 5.41 (5.55). FT-IR (ATR, $\tilde{\nu}_{\text{max}}/\text{cm}^{-1}$): 3059 (w, C-H_{ar}), 2961,

2902, 2867 (w, C-H_{alif}), 1603, 1513 (m, C-C_{ar} a C_{ar}-N). UV-VIS (acetonitrile, λ/nm , $1.10^{-5} \text{ mol.L}^{-1}$): 315, 531.

S1.3 Single-crystal diffraction experiments

Data collection for all studied structures were performed on an Eulerian 4-circle diffractometer Stoe STADIVARI with a Dectris Pilatus 300K detector and with a microfocus source (Cu-K α , $\lambda = 1.54186 \text{ \AA}$) at 100 K using a nitrogen gas open-flow cooler Cobra from Oxford Cryosystems. All studied structures are depicted in Table 1. Data reduction was processed by Stoe X-Red and cell refinement by Stoe X-Area³. Absorption correction was performed by LANA.⁴ Crystal structures of all complexes were solved by intrinsic phasing with program ShelXT⁵ using OLEX2⁵ and were subsequently refined by using SHELXL⁵. Positions of all hydrogen atoms were geometrically optimized and constrained to ride on their parent atoms, with $d(\text{C-H}) = 0.93 \text{ \AA}$ (aromatic), 0.96 \AA (methyl) and 0.97 \AA (CH₂ groups) with $U_{\text{iso}}(\text{H}) = 1.2U_{\text{eq}}(\text{C})$ for all hydrogen atoms except for methyl group where $U_{\text{iso}}(\text{H}) = 1.5U_{\text{eq}}(\text{C})$. All non-hydrogen atoms were refined with anisotropic thermal parameters. The studied structures contain voids of disordered solvent molecules (**1**, **3** and **8**), therefore, a solvent mask implemented in the program OLEX2 was applied to account for embedded solvent molecules. In the crystal structure **6** the BPh₄⁻ anion was disordered with ratio 1:1 and in the crystal structure **7** the ClO₄⁻ with ratio 3:1.

S1.4 Magnetic measurements

All herein reported magnetic measurements were performed on a MPMS-XL7 magnetometers (Quantum Design). For standard magnetic as well as for photomagnetic experiments, the temperature dependent magnetization was recorded at $B_{\text{DC}} = 0.1 \text{ T}$ as an external magnetic field. The temperature sweeping rate was 1 K min^{-1} (standard measurements in the dark) or 0.3 K min^{-1} (photomagnetic experiments) and it was the same for cooling and for heating modes. Every temperature data point was stabilized for 2 minutes before the measurement. Gelatine capsule (standard measurements in the dark) was used as sample holders in the temperature range $1.8 \leftrightarrow 400 \text{ K}$. The very small diamagnetic contribution of the gelatin capsule was negligible to the overall magnetization, which was dominated by sample. The diamagnetic corrections of the molar magnetic susceptibilities were applied using Pascal's constants.⁷ The photomagnetic measurements were performed by using a diode-pumped solid-state lasers (DPSS) Kvant ($\lambda = 637 \text{ nm}$ or 532 nm , 300 mW) coupled through an optical fiber to the cavity of a MPMS SQUID and the power on the sample surface was adjusted to 10 mW cm^{-2} . For the photomagnetic experiments, the small amount of sample was introduced onto transparent tape and mounted into the sample holder. The exact weight of samples (ca 0.1 mg) was obtained by weighting and also verified by comparison of thermal χT . vs T curve with more accurately weighed sample of the same compound. After the cooling to 5 K , the sample was irradiated and the change in magnetization was followed. When the saturation point had been reached, the light was switched off, the temperature was increased at a rate of 0.3 K min^{-1} , and the magnetization was measured at 1 K intervals. We observed the most intense increase of magnetic moment under

the red-light irradiation (637 nm). T(LIESST) value was determined from the minimum of the $\partial(\chi T)/\partial T$ vs T curve for the relaxation process.

S1.5 Electrochemistry

Electrochemical measurements were carried out using a three-electrode electrochemical cell system for cyclic voltammetry (CV). The reference electrode (RE), Ag|AgCl|1M LiCl, was separated from the measured solution by a salt bridge. The working electrode (WE) was glassy carbon disc electrode ($A = 2 \text{ mm}^2$). The counter electrode (CE) was a platinum wire in the shape of a spiral with area ca $175 \times$ higher than area of WE. Oxygen was removed from the solution by passing a stream of argon for at least 15 min. before the start of experiments and then at least 1 min before each repetition. All electrochemical experiments were performed at $24 \pm 1 \text{ }^\circ\text{C}$ in 0.1 M anhydrous tetrabutylammonium hexafluorophosphate (TBAPF₆, for electrochemical analysis $\geq 99.0\%$, Sigma-Aldrich) dissolved in dry acetonitrile (Sigma-Aldrich). Acetonitrile was dried over molecular sieve (Sigma-Aldrich) for at least 5 days prior experiments. TBAPF₆ was dried before beginning of each experimental day for 30 minutes in the vacuum oven and kept in a desiccator throughout the day.

S2. Spectral characterisation

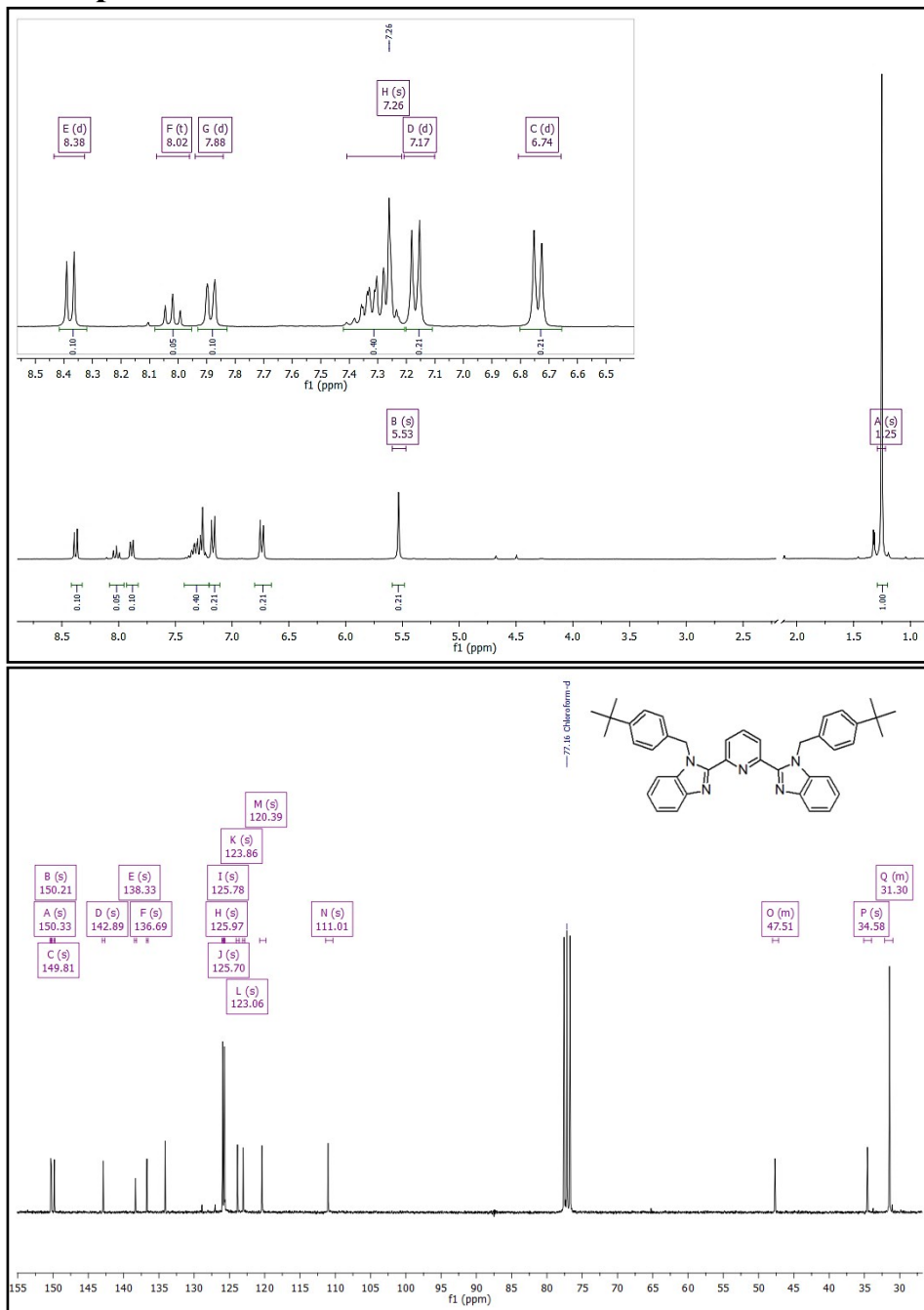


Figure S1 ^1H NMR (up) and ^{13}C NMR (down) of ligand **L2**.

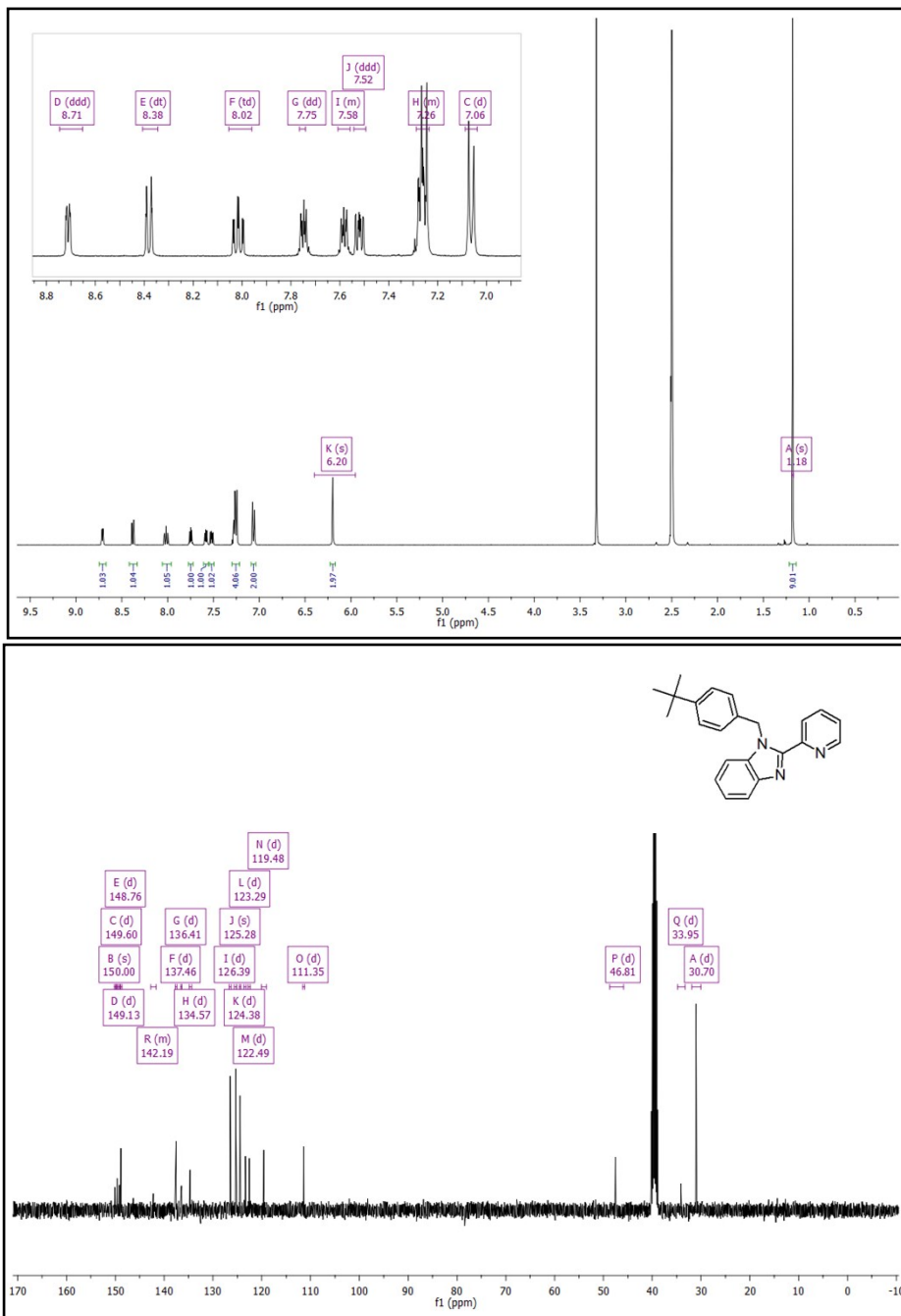
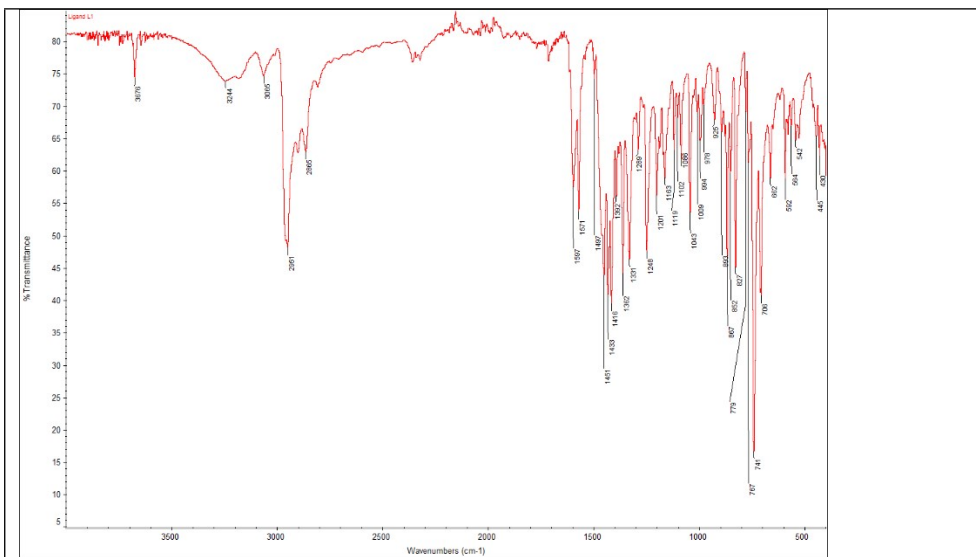
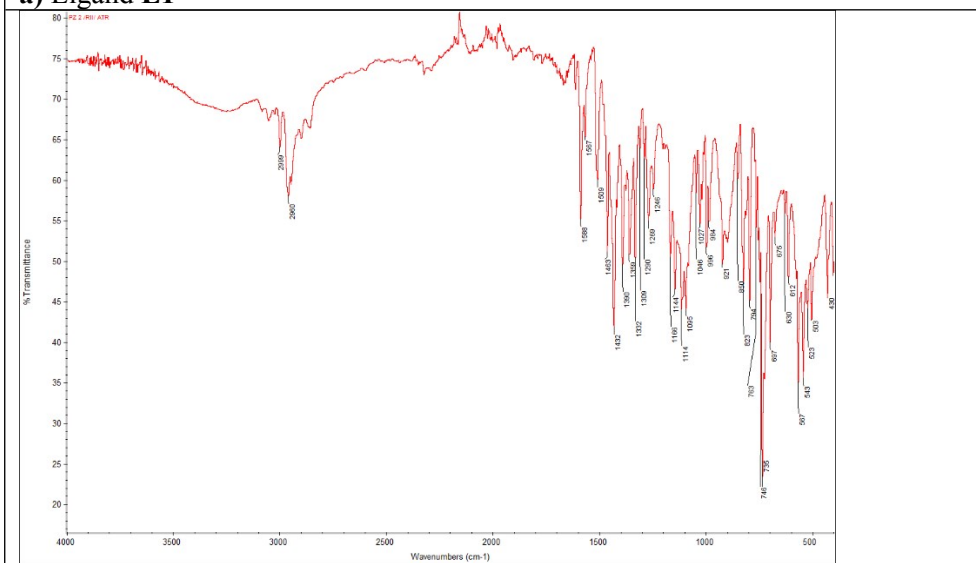


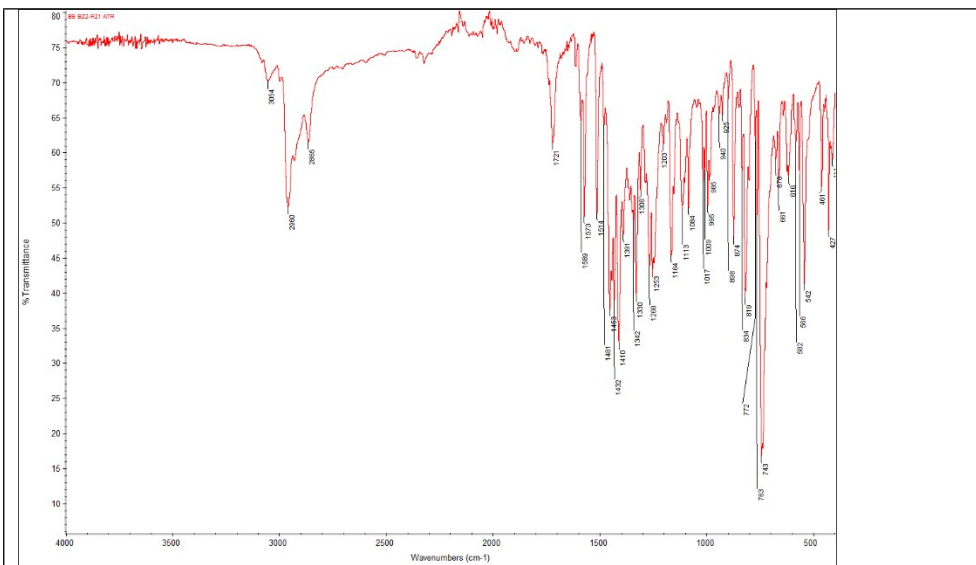
Figure S2 ^1H NMR (up) and ^{13}C NMR (down) of ligand **L3**.



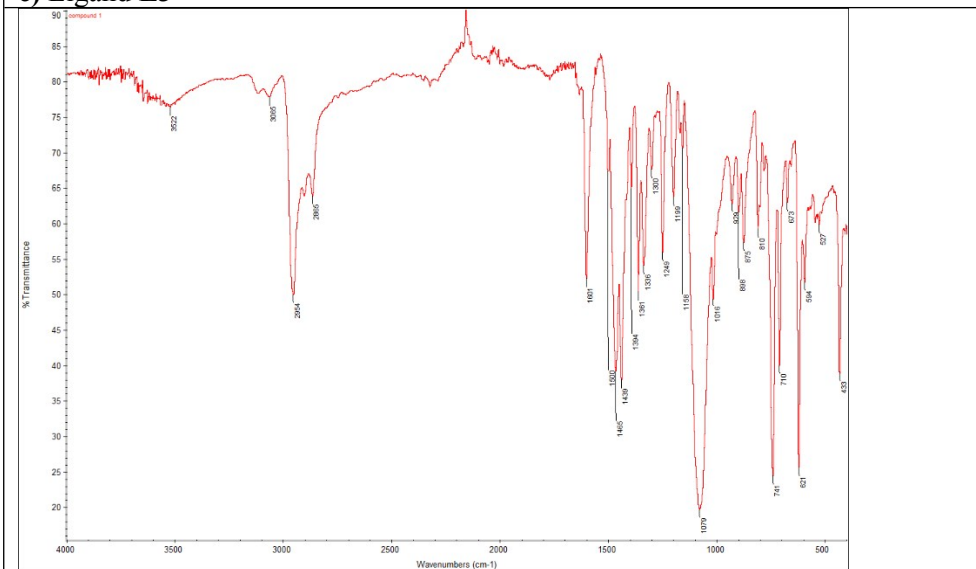
a) Ligand L1



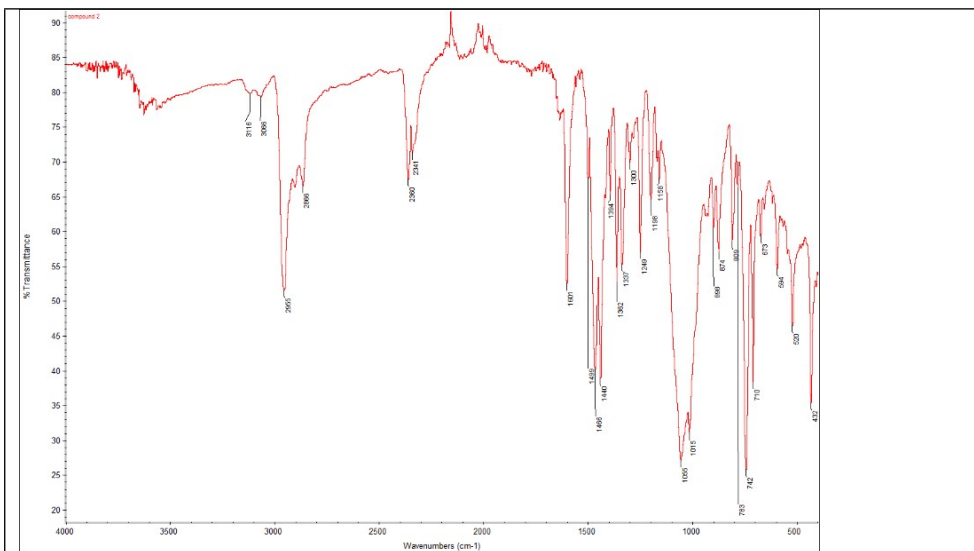
b) Ligand L2



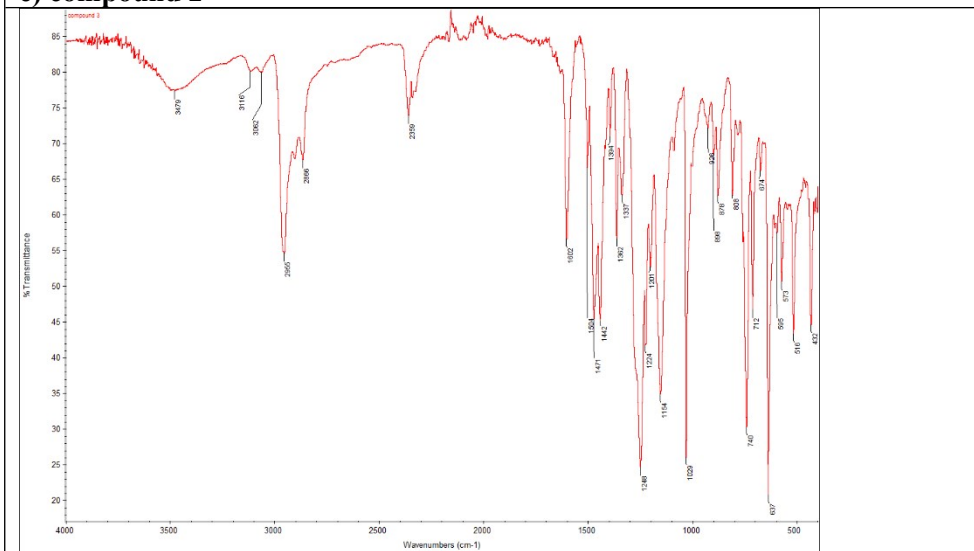
c) Ligand L3



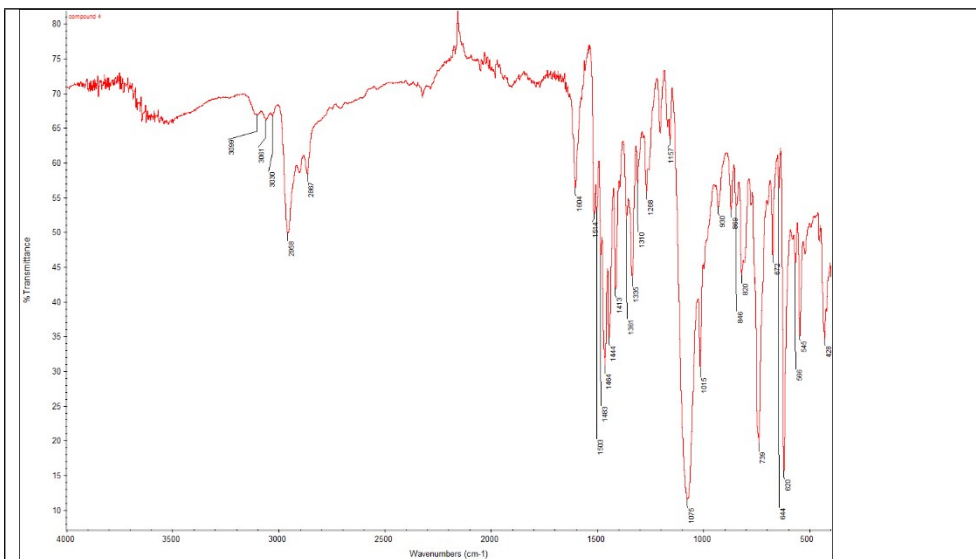
d) compound 1



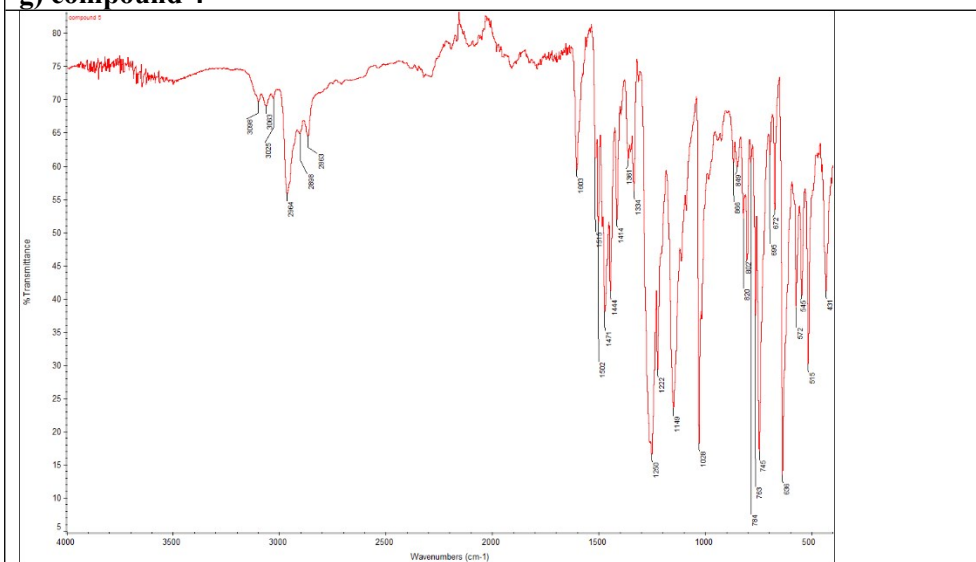
e) compound 2



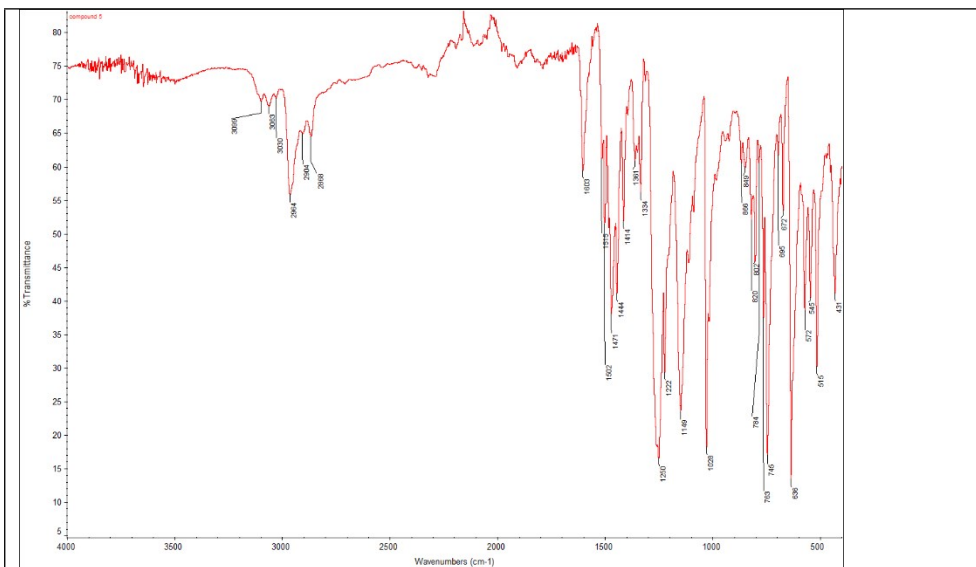
f) compound 3



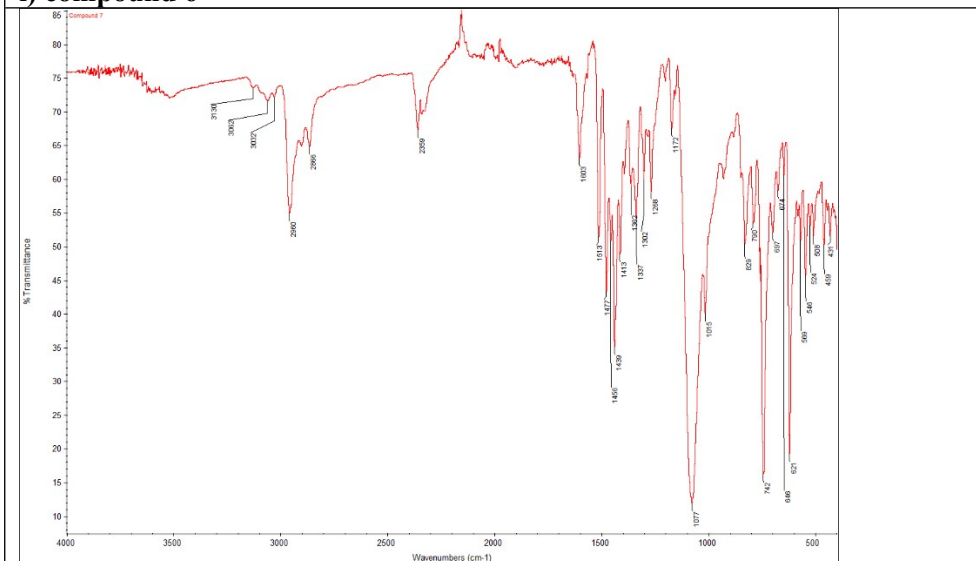
g) compound 4



h) compound 5



i) compound 6



j) compound 7

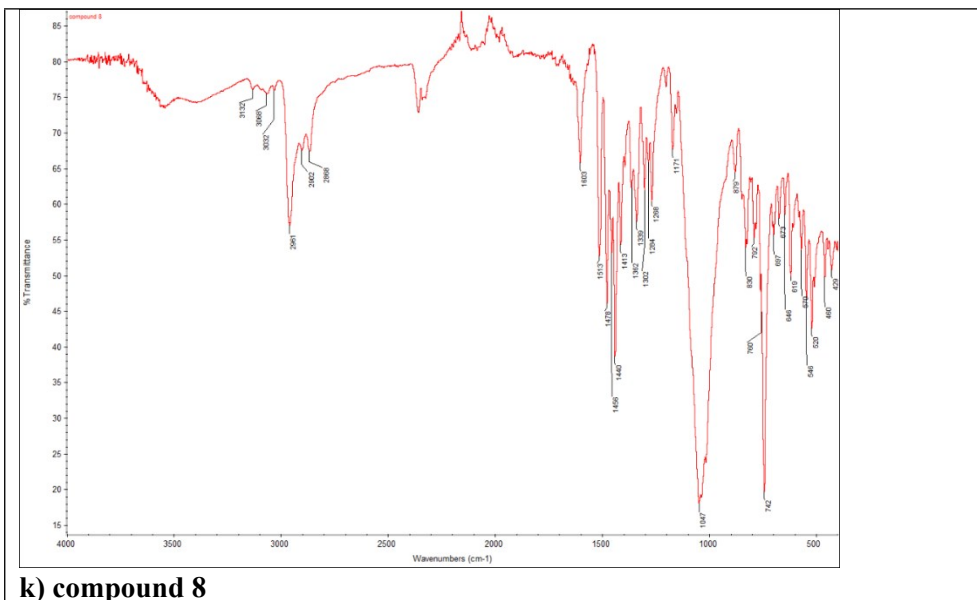


Figure S3 FT-IR spectra of reported ligands and compounds 1-8.

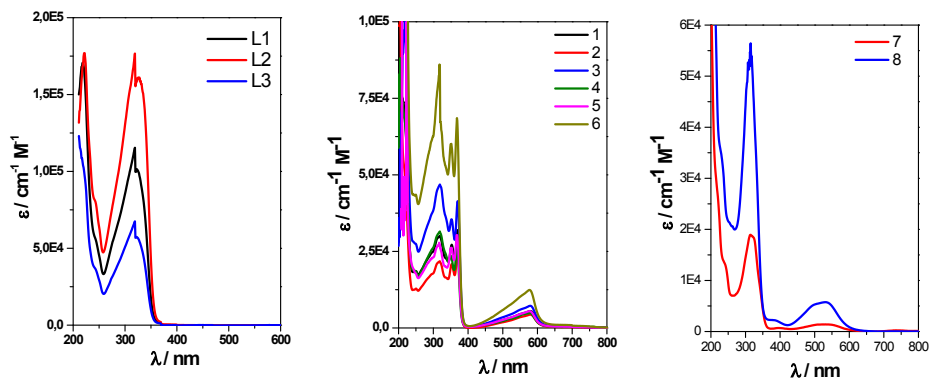
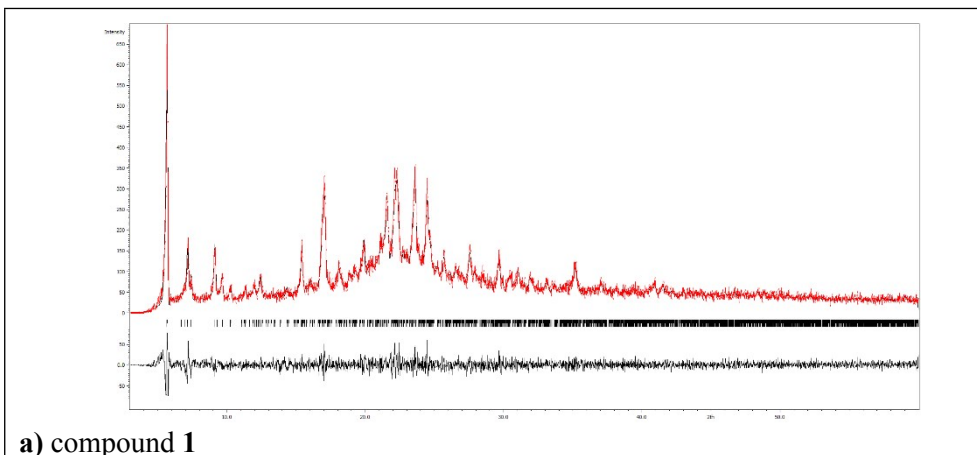
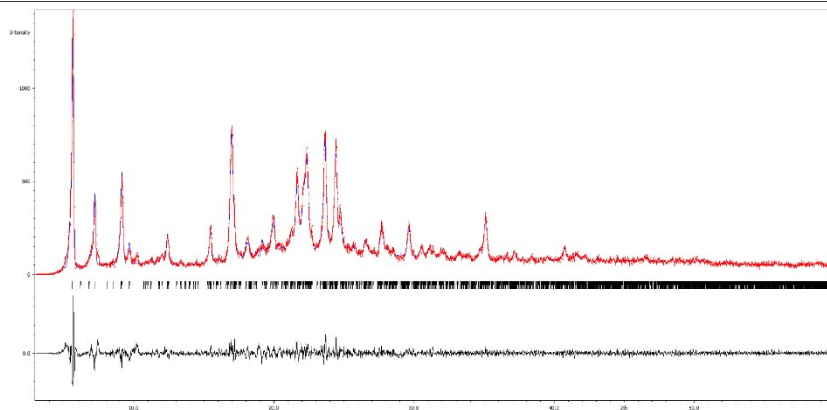
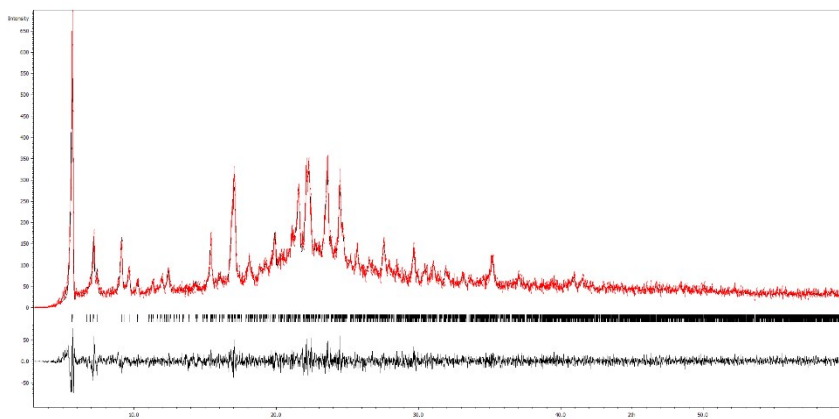


Figure S4 UV-VIS spectra of reported ligands and compounds 1-8 in acetonitrile ($c \approx 10^{-5} \text{ mol} \cdot \text{dm}^{-3}$).

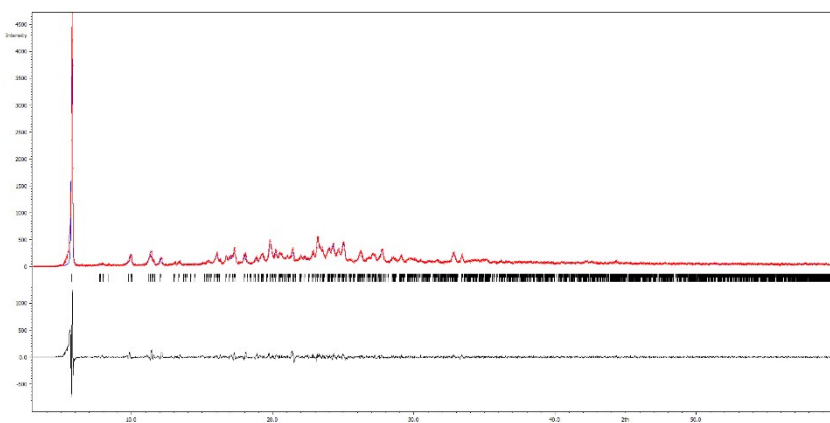




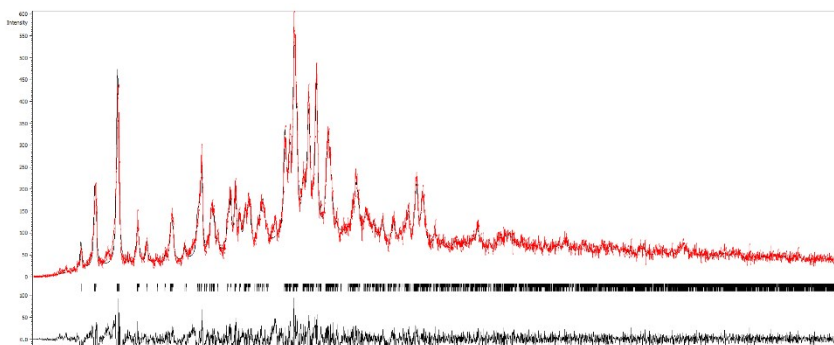
b) compound 2

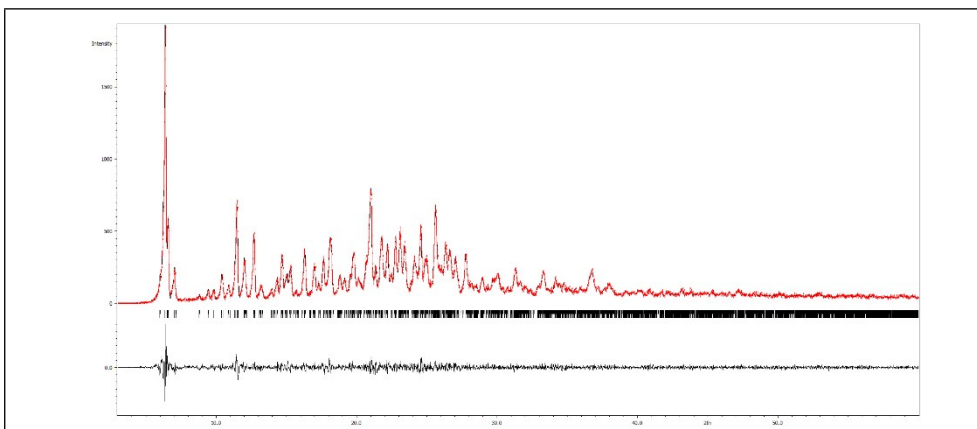


c) compound 3

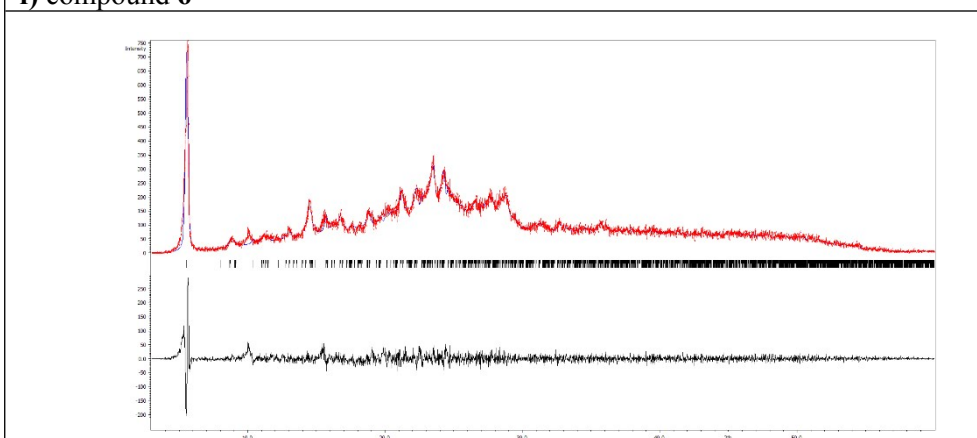


d) compound 4

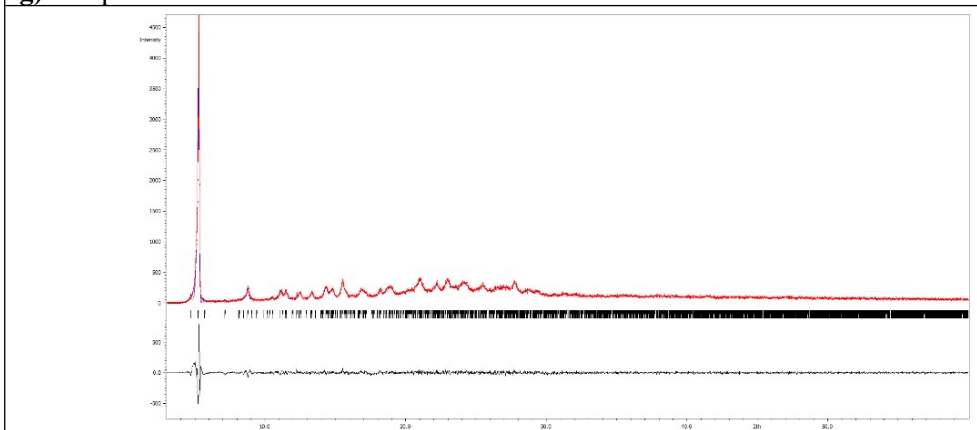




f) compound 6



g) compound 7



h) compound 8

Figure S5 X-ray powder measurements of compounds 1-8.

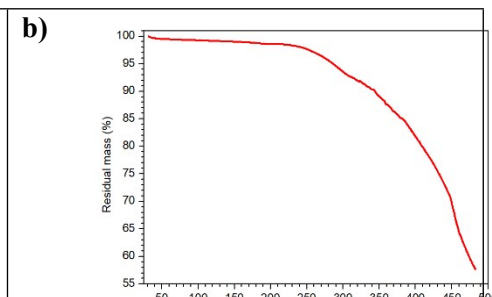
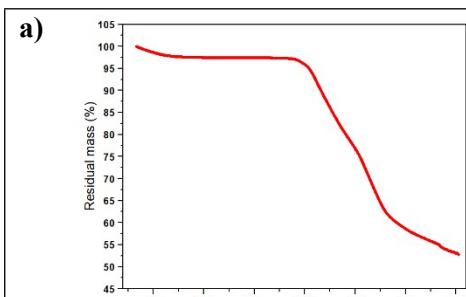


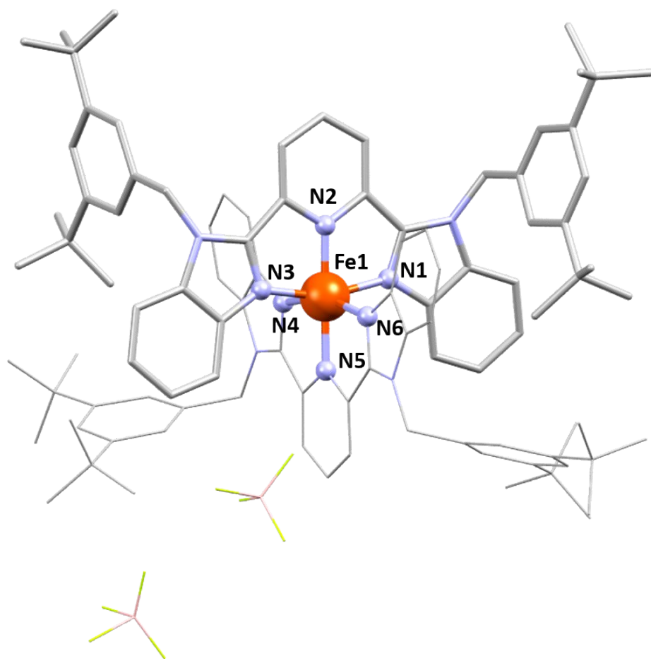
Figure S6 Thermogravimetric analysis of compound **a) 7** and **b) 8**.

S3. Supplementary structural information

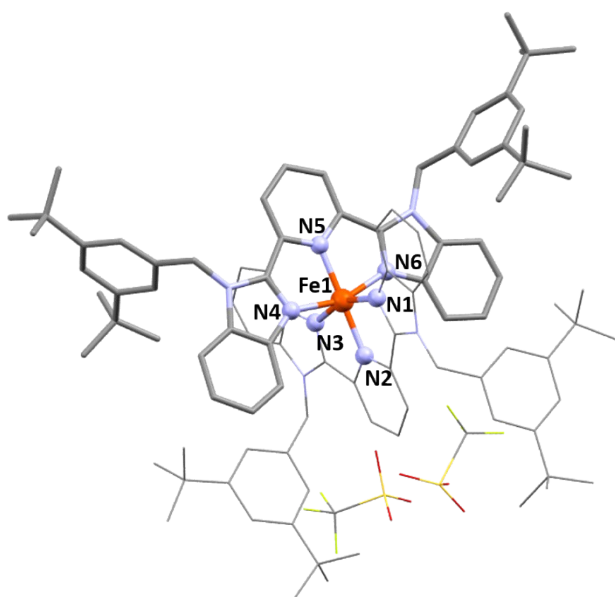
	1	2	3	4	5	6	7	8 Fe1	8 Fe2
Fe-N1	1.966(3)	1.959(4)	1.976(4)	1.956(3)	1.97(1)	1.968(5)	1.965(4)	1.943(8)	1.974(7)N13
Fe-N2	1.915(3)	1.836(3)	1.896(5)	1.909(3)	1.92(1)	1.906(3)	1.995(3)	2.013(8)	2.002(8)N15
Fe-N3	1.976(3)	1.970(5)	1.975(5)	1.968(3)	1.98(1)	1.977(5)	1.954(4)	1.952(7)	1.950(6)N11
Fe-N4	1.905(3)	1.968(3)	1.959(4)	1.964(4)	1.96(1)	1.970(5)	2.021(4)	1.989(7)	1.963(8)N12
Fe-N5	1.905(3)	1.889(4)	1.915(5)	1.908(3)	1.90(1)	1.910(4)	2.002(4)	1.978(7)	2.009(7)N10
Fe-N6	1.971(2)	1.981(3)	1.976(4)	1.965(4)	1.96(1)	1.968(5)	1.999(3)	1.999(7)	1.984(8)N14
Σ /°	83	82	83	83	86	88	73	74	72
Θ /°	270	272	273	270	280	270	137	131	141
ϕ /°	177.6(1)	179.1(2)	179.1(2)	177.8(1)	177.7(6)	177.8(2)	-	-	-
θ /°	89.8(1)	88.7(2)	87.1(2)	85.8(1)	88.3(6)	81.2(2)	-	-	-
α_{avg} /°	80.5(1)	80.5(2)	80.4(2)	80.4(1)	79.8(6)	80.5(2)	80.1(2)	79.7(3)	80.6(3)
φ_{avg} /°	160.9(1)	161.1(2)	160.8(2)	160.9(1)	160.2(6)	160.8(2)	-	-	-
S(OC-6)	1.900	1.907	1.923	1.915	2.058	1.947	0.906	0.928	0.876
S(TPR-6)	12.290	12.533	12.495	11.629	11.993	12.102	13.691	13.977	13.835
S(PPY-6)	23.759	24.241	24.171	23.511	23.304	23.120	25.554	25.763	24.975
S(JPPY-6)	27.695	28.193	28.003	27.464	27.167	26.824	28.684	29.012	28.059
S(HP-6)	33.760	34.194	34.050	34.117	33.854	32.858	26.493	26.595	26.360

Table S1 Table of selected bond distances of **1-8** at 100 K and results of the SHAPE calculations for coordination polyhedra **1-8**. PP (D_{5h}) – pentagon; vOC (C_{4v}) vacant octahedron; TBPY (D_{3h}) trigonal bipyramid; SPY (C_{4v}) spherical square pyramid; JTBPY (D_{3h}) Johnson trigonal bipyramid.

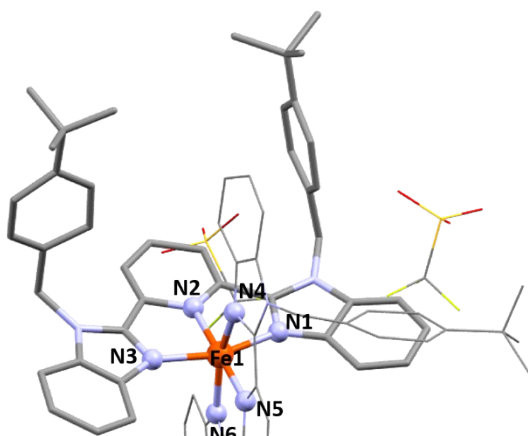
a)



b)



c)



d)

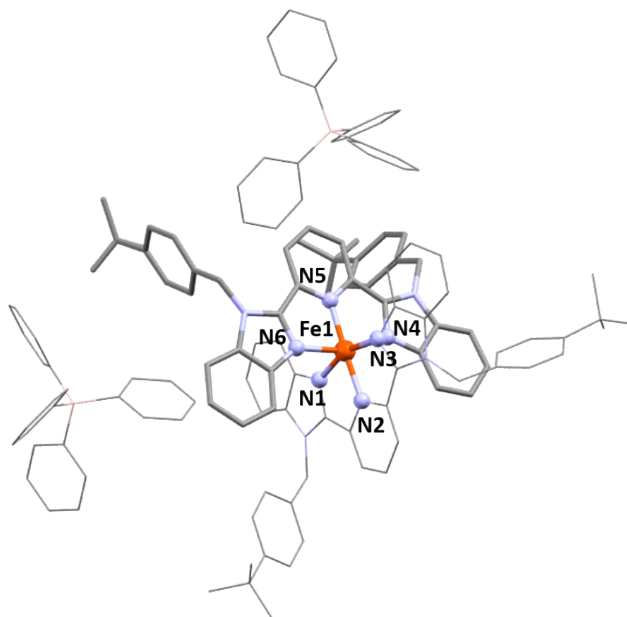


Figure S7 The asymmetric units of **a) 2**, **b) 3**, **c) 5** and **d) 6**. The hydrogen atoms and lattice solvent molecules were omitted for clarity. Colour code: C- grey; N- blue; O- red; S- yellow; Fe- orange; B- pink; Cl- green, F- light green.

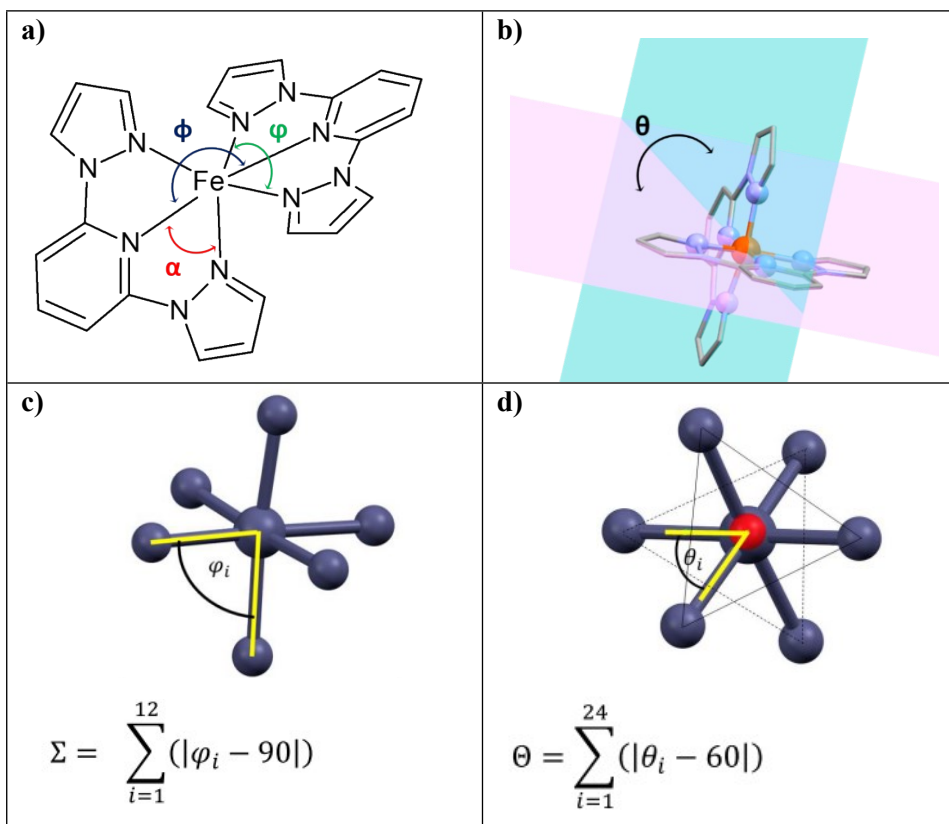


Figure S8 Schematic representation of the angular metric parameter. **a)** α – bite angle (average value of four $N_{im}-Co-N_{py}$); ϕ – trans angle $N_{py}-Co-N_{py}$; φ - clamp angle (average value of two $N_{pz}-Fe-N_{pz}$); **b)** θ - dihedral angle between the least squares planes of the two bpp moieties coordinating the same metal center; **c)** Calculation of distortion parameters Σ , where φ_i is one of 12 cis angles of corresponding hexacoordinated polyhedron; **d)** Calculation of distortion parameters Θ , where θ_i is one of 24 dihedral angles measured on the projection of two triangular faces of the hexacoordinated polyhedron along with their common pseudo-threefold axis.

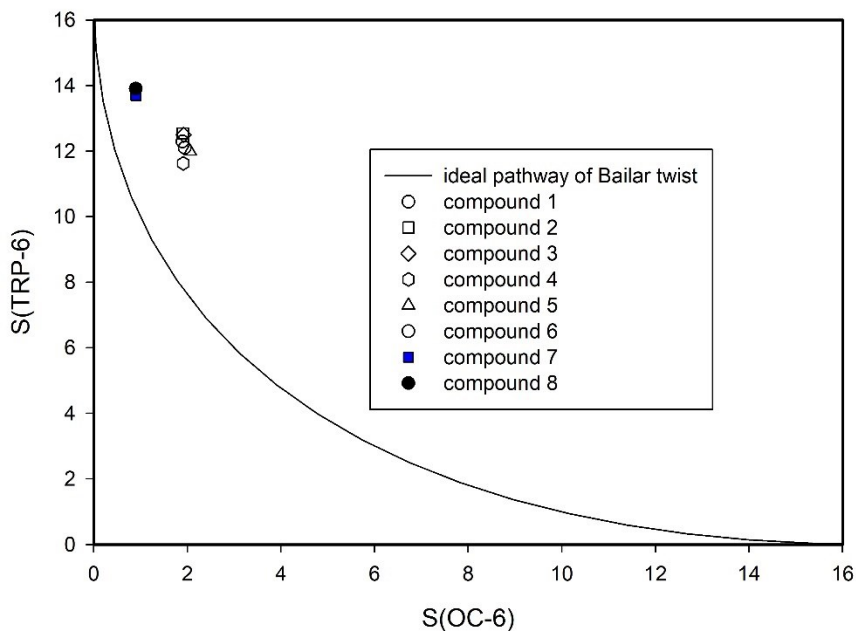


Figure S9 Shape map of coordination polyhedra in **1-8**. Solid line represents ideal Bailar twist pathway between octahedral S(OC-6) and trigonal prism S(TRP-6) geometry.

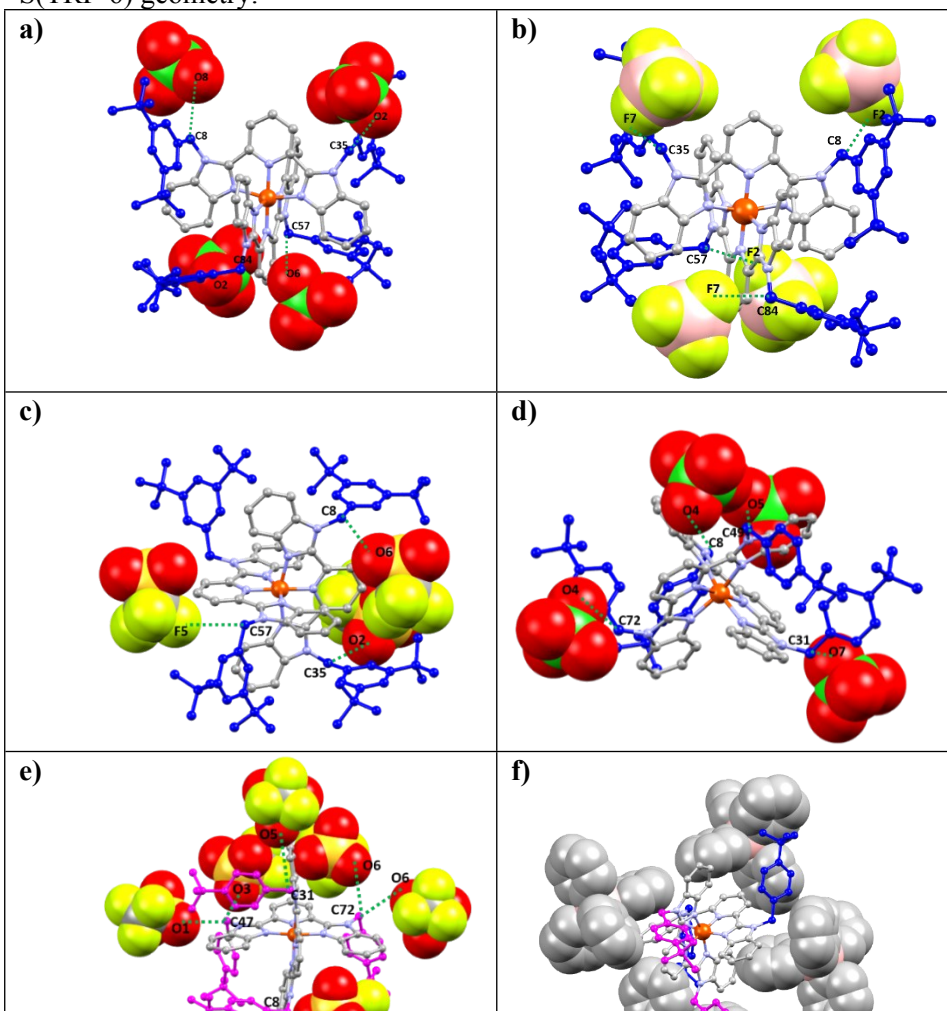


Figure S10 Complex cations of **1-6** and alignment of corresponding counter anions in their close environment. The 3,5-bis(*t*-butyl)benzyl and 4-(*t*-butyl)benzyl substituents are visualised in blue and magenta colour according their orientation in the opposite and in the same orientation, respectively, with respect to 2,6-bis(benzimidazole-1-yl)pyridine moiety. The distances of electronegative O or F atoms and methylene carbon atoms are: **a)** compound **1**: O2...C35=3.095(4) Å; O2...C84=3.116(5) Å; O6...C8=3.340(5) Å; O6...C57=3.121(5) Å; **b)** compound **2**: F5...C35=2.986(9) Å, F2...C8=3.222(7) Å, F2...C57=3.17(1) Å, F7...C84=3.011(9) Å; **c)** compound **3**: C35...O2=3.54(2) Å, F5...C57=3.87(1) Å, O6...C8=3.31(1) Å; **d)** compound **4**: C8...O5=3.521(7) Å, O4...C72=3.169(6) Å, O4...C49=3.286(6) Å, O7...C31=3.243(6) Å; **e)** compound **5**: C72...O6=3.81(2) Å, O6...C72=3.54(2) Å, O5...C31=4.55(2) Å, O2...C8=3.55(2) Å, O1...C49=3.30(2) Å, O3...C49=3.54(2) Å, F5...C8=3.31(2) Å.

S4. Magnetic measurements

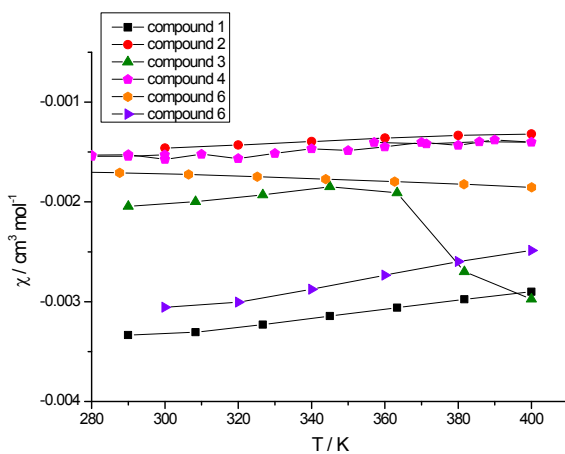


Figure S11 Magnetic properties of **1-6**.

Table S2 Comparison of magnetic behaviour herein reported compounds with literature.

Compounds	Magnetic behaviour	Ref.
[Fe(bzimpy) ₂](ClO ₄) ₂ ·0.25H ₂ O	SCO $T_{1/2\uparrow} = 409$ K, $T_{1/2\downarrow} = 397$ K	7
[Fe(bzimpy) ₂](BPh ₄) ₂ ·4H ₂ O	SCO $T_{1/2} = 300$ K	8
[Fe(bzimpy) ₂](BPh ₄) ₂	HS	8
[Fe(bzimpy- _{1H}) ₂]·H ₂ O	SCO	9

	$T_{1/2\uparrow} = 424 \text{ K}$	
[Fe(Me-bzimpy) ₂](ClO ₄) ₂	LS	10
[Fe(Pr-bzimpy) ₂](ClO ₄) ₂	LS	10
[Fe(t-bu ₂ Bz-bzimpy) ₂](ClO ₄) ₂	LS	10
Compounds 1-6	LS	this work
bzimpy= 2,6-bis(1 <i>H</i> -benzimidazol-2-yl)pyridine; Me-bzimpy= 2-[6-(1 <i>H</i> -benzimidazol-2-yl)-pyridin-2-yl]-1-methyl-1 <i>H</i> -benzimidazole; Pr-bzimpy=2-[6-(1 <i>H</i> -benzimidazol-2-yl)-pyridin-2-yl]-1-isopropyl-1 <i>H</i> -benzimidazole; t-bu ₂ Bz-bzimpy= 2-[6-(1 <i>H</i> -benzimidazol-2-yl)-pyridin-2-yl]-1(3,5-di-tert-butyl-benzyl)-1 <i>H</i> -benzoimidazole		

References

1. a) A. W. Addison and P. J. J. Burke, *Heterocycl. Chem.*, 1981, **18**, 803–805. b) C. G. Wahlgren and A. W. J. Addison, *Heterocycl. Chem.*, 1989, **26**, 541–543.
2. B. Brachňaková, S. Matejová, J. Moncol, R. Herchel, J. Pavlik, E. Moreno-Pineda, M. Ruben and I. Šalitraš, *Dalton Trans.*, 2020, **49**, 1249-1264.
3. STOE & Cie GmbH (2018). X-Area, software package for collecting single-crystal or multi-domain crystal data on STOE area-detector diffractometers, for image processing, for the correction and scaling of reflection intensities and for outlier rejection Darmstadt.
4. J. Koziskova, F. Hahn, J. Richter and J. Kozisek, *Acta Chimica Slovaca*, 2016, **9**, 136–140.
5. G. M. Sheldrick, *Acta Crystallogr. Sec. A Found Adv.*, 2015, **71**, 3-8.
6. O. V. Dolomanov, L. J. Bourhis, R. J. Gildea, J. A. K. Howard and H. Puschmann, *J. Appl. Crystallogr.*, 2009, **42**, 339-341.
7. R. Boča, *Theoretical Foundations of Molecular Magnetism*, Elsevier, Amsterdam, 1999.
8. R. Boča, M. Boča, L. Dlháň, K. Falk, H. Fuess, W. Haase, W. Linert, B. Papánková and R. Werner, *Inorg. Chem.*, 2001, **40**, 3025–3033.
9. R. Boča, P. Baran, L. Dlháň, J. Šima, G. Wiesinger, F. Renz and W. Linert, *Polyhedron*, 1997, **16**, 47–55
10. R. Boča, F. Renz, M. Boča, H. Fuess, W. Haase, G. Kickelbick, W. Linert and M. Vrbová-Schikora, *Inorg. Chem. Comm.*, 2005, **8**, 227–230.
11. C. Rajnák, J. Titiš, O. Fuhr, M. Ruben and R. Boča, *Polyhedron*, 2017, **123**, 122–131.